Talanta 81 (2010) 1560–1567

Contents lists available at ScienceDirect

Talanta

journal homepage: www.elsevier.com/locate/talanta

Highly sensitive homogenous immunoassay of cancer biomarker using silver nanoparticles enhanced fluorescence correlation spectroscopy

Lichuan Tang, Chaoqing Dong, Jicun Ren*

College of Chemistry and Chemical Engineering, State Key Laboratory of Metal Matrix Composites, Shanghai Jiaotong University, 800 Dongchuan Road, Shanghai, 200240, PR China

ARTICLE INFO

Article history:
Received 18 December 2009
Received in revised form 1 March 2010
Accepted 2 March 2010
Available online 7 March 2010

Keywords:
Silver nanoparticle
Fluorescence correlation spectroscopy
Fluorescence enhancement
Homogeneous immunoassay
Alpha fetal protein

ABSTRACT

In this paper, we developed a highly sensitive homogeneous immunoassay by combining fluorescence correlation spectroscopy (FCS) with silver nanoparticles (SNPs)–antibody conjugates as probes. We first synthesized 14 nm SNPs in aqueous solution and then modified SNPs with 11-mercaptoundecanoicacid (MUA) via SNP–S bond. Resonance light scattering correlation spectroscopy (RLSCS) was utilized to characterize SNPs and MUA–functionalized SNPs (MUA–SNPs). The immune reaction of alpha fetal protein (AFP) antigen and its antibody was used as a reaction model and AFP labeled with Alexa Fluor 647 was used as the tracer antigen in homogeneous competitive immunoassay. We observed that the antigen–antibody complexes showed the significant increase in the diffusion times and fluorescence intensity compared to free dye-labeled antigen. On the advantages of the effects of SNPs on fluorescence enhancement and diffusion time, the homogeneous competitive immunoassay was performed by the two-component model analysis of FCS. Under the optimal condition, the detection limit was 1.5 pM and the linear range was from 6 pM to 60 pM ($R > 0.99$). This assay was successfully applied for the determination of the AFP level in human serum samples, the relative standard deviation was about 5%, and the recoveries were over 90%.

1. Introduction

Currently, immunoassay is widely used in clinical diagnosis, food and environmental analysis and biological and biomedical studies [1–5]. The conventional heterogeneous immunoassays are considered to be labor intensive and time-consuming due to the requirements of tedious separation and washing steps before the signal measurement [6]. Homogeneous immunoassay is an attractive alternative to conventional heterogeneous immunoassays since it can directly determine analytes (antigen or antibody) in the immune reaction mixture, and this method is usually simple, fast and amenable to miniaturization and automation [7,8]. To date, several analytical methods have been used in homogeneous immunoassays, which mainly include fluorescence polarization [8], fluorescence resonance energy transfer (FRET) [9], and fluorescence correlation spectroscopy (FCS) [10–12]. However, most of the current homogeneous immunoassays are generally less sensitive than their heterogeneous counterparts due to their high background noise.

FCS is a single molecule detection (SMD) technique based on the time-averaging fluctuation analysis for observation of the diffusion of molecules (or particles) in the small detection volume [13–15]. On the advantages of high sensitivity, extremely small sample requirement and short analysis time, FCS currently becomes an all-purposed and powerful technique to study binding interactions [16,17], especially in homogeneous immunoassays [10,11,18]. Nevertheless, FCS system is still difficult to be utilized for clinical diagnoses since the specificity and sensitivity were unsatisfactory. So far, two strategies are used to overcome this limitation: (1) Use of fluorescence cross-correlation spectroscopy (FCCS) model. In this strategy, FCCS model can overcome the limitation abovementioned and increase the detection sensitivity and selectivity [10,19], but this model requires the complicated two laser optical system and two-color labeling process. (2) Amplification of the molecular weight difference between antigen and immune complex. In general, to distinguish two components in FCS assay, their characteristic diffusion times must differ by a factor of at least 1.6 [20]. Sandwich immune strategy was used to increase the molecular weight of the immune complex [11,21], but the sensitivity was restricted by the limited diffusion difference and the interference of multiple antibodies. In competitive immunoassay, only few little antigens and large antibodies match such requirement of molecular weight difference [17,18,22].

Gold nanoparticles (GNPs) and silver nanoparticles (SNPs) as probes are widely used in cell imaging [23–25], DNA hybridization detection [7,26–29], proteins interaction [30–32], due to their extremely strong absorption and light scattering in the plasmon resonance wavelength regions. Recently, some groups

* Corresponding author. Tel.: +86 21 54746001; fax: +86 21 54741297.
E-mail address: jicunren@sjtu.edu.cn (J. Ren).

0039-9140/$ – see front matter © 2010 Elsevier B.V. All rights reserved.
doi:10.1016/j.talanta.2010.03.002

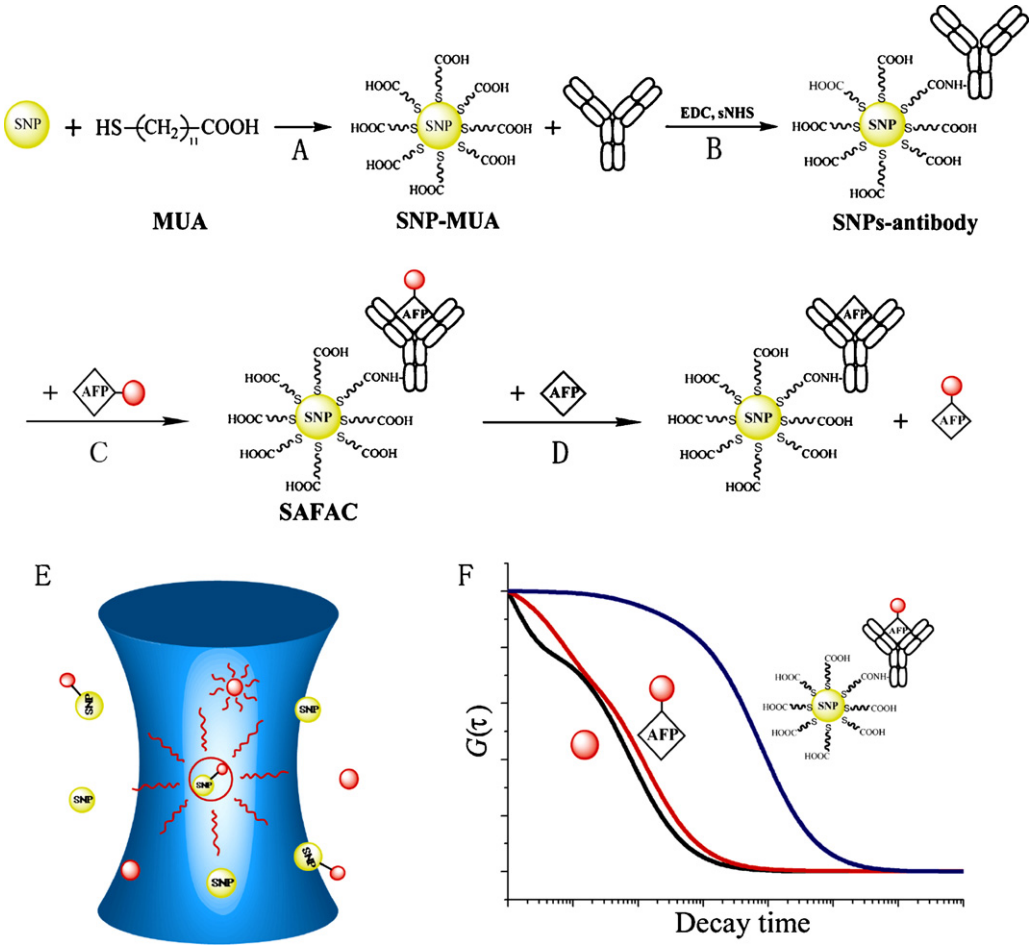

Fig. 1. Schematic illustration of homogeneous competitive immunoassay using silver nanoparticles (SNPs) enhanced fluorescence correlation spectroscopy (FCS). (A) Surface modification of SNPs with MUA. (B) Conjugation of SNP–MUA with antibody. (C) The immune reaction of SNP–antibody conjugations with dye-labeled antigen. (D) The competitive immune reaction. (E) and (F) The principle of the competitive immunoassay based on FCS.

found that some metal nanoparticles such as SNPs were used to increase the fluorescent intensity in the metal–fluorophore system [33–37]. This effect is called as metal-enhanced fluorescence (MEF) [28,33,38]. The enhancement efficiency is proved to be closely related with the distance between metal nanoparticles and fluorophores, and generally, about 10 nm is considered to be an optimal value for the most efficient MEF [33,39]. But, in the case of large proteins such as green fluorescence protein (GFP) [40] and immune reaction system [41], SNPs also show MEF coupled with fluorophores.

In this paper, we developed a highly sensitive homogeneous immunoassay by using silver nanoparticles enhanced fluorescence correlation spectroscopy (FCS). The principle and procedure of this immunoassay are shown in Fig. 1. In the immunoassay, SNPs served two functions. The one was to enlarge the molecule weight difference between the immunocomplex and antigen, and another was to enhance the fluorescent intensity of fluoroprobes. We first synthesized 14 nm SNPs in aqueous solution and then modified SNPs with 11-mercaptoundecanoicacid (MUA) via SNP–S bond. MUA–SNPs were covalently linked with antibody. Resonance light scattering correlation spectroscopy (RLSCS) [42] was utilized to characterize MUA–functionalized SNPs (MUA–SNPs) and SNPs–antibody conjugates. The immune reaction of alpha fetal protein (AFP) antigen [43] and its antibody was used as a reaction model in this study. AFP labeled with Alexa Fluor 647 was used as the tracer antigen in homogeneous competitive immunoassay. In the FCS based competitive immunoassay, we used the two-component analysis model [11,17,18,22]. Under the optimal condition, the detection limit was 1.5 pM AFP and the linear ranges were from 6 pM to 60 pM. This assay was successfully applied for the determination of the AFP level in human serum samples.

2. Experimental

2.1. Reagents and instruments

Sodium citrate trihydrate (≥99.9%), $AgNO_3$ (≥99.9%), $NaBH_4$ (≥98%), and poly(ethylene glycol) (PEG. 2 kDa) were products of Sinophram Chemical Reagent Co. (Shanghai, China). 11-Mercaptoundecanoic acid (MUA, ≥95%), and 1-ethyl-3-(3-dimethylaminopropyl)-carbodiimide hydrochloride (EDC, ≥99%) and N-hydroxysulfosuccinimide (Sulfo-NHS, ≥98.5%) were purchased from Sigma–Aldrich. Mouse anti-human monoclonal alpha fetal protein antibodies and AFP antigen protein were provided by Beijing North Institute of Biological Technology (Beijing, China). Alexa Fluor 647 was obtained from Invitrogen Co. (USA). All solutions were prepared using ultra-pure water (18.2 MΩ) obtained from the Millipore Simplicity System (Millipore, Bedford, MA, USA).

2.2. Preparation of Alexa Fluor 647-labeled antigen

The antigen (AFP) was labeled with the succinimidyl esters fluorescence dye (Alexa Fluor 647) according to the manufacturer's instruction. The amine-reactive succinimidyl ester form of the dye

and antigen were dissolved in sodium carbonate-sodium bicarbonate buffer solution (pH 9.4, containing 20 mL of 0.01 M Na_2CO_3 and 80 mL of 0.01 M $NaHCO_3$) at a molar ratio of 1/1 for 24 h resulting in the covalent attachment of the dye to the lysine and end-terminal amine groups on the antigen. The dye-labeled antigen was ultrafiltrated three times to remove unbound dye with PBS (pH 7.4, containing 81 mL of 0.01 M Na_2HPO_4 and 19 mL of 0.015 M NaH_2PO_4). The residue was dissolved in PBS and stored in the dark at 4 °C and working dilutions were made daily.

2.3. Synthesis of SNPs

Synthesis of SNPs was performed according to the procedure described in the reference [24,44]. Briefly, we first mixed 96 mL of 0.25 mM $AgNO_3$ solution with 1 mL 30 mM sodium citrate and stirred this mixture constantly at 30 °C. And then, 3 mL of 10 mM $NaBH_4$ stored in ice was added into the mixed solution, and the color of the solution changed from colorless to bright yellow. We kept up stirring the mixed solution at room temperature for 30 min. The as-prepared SNPs were characterized by UV–vis absorption spectroscopy, resonance scattering spectroscopy and transmission electron microscopy, respectively.

2.4. Modification of SNPs with MUA

Twenty five micrograms of MUA in ethanol was added into 1 mL SNPs solution (about 1.4 nM) and then stirred for 30 seconds. This mixture was kept up reacting at room temperature for 2–4 h. SNPs–MUA was washed three times with PBS by centrifugation (12,000 rpm, 30 min, at 4 °C). SNPs–MUA was stored at 4 °C for further use.

2.5. Conjugation of SNPs with antibody

Conjugation of SNPs with antibody was carried out using EDC and Sulfo-NHS as linking reagents according to the protocol described in the reference [24]. Briefly, 8 μg EDC and 39 μg Sulfo-NHS were first added into 1 mL SNP–MUA solution (2.8 nM) to amidate carboxyl terminus of MUA on SNPs for 40 min to prepare SNP–MUA@NH nanoparticles in the presence of 0.05% PEG (w/v). PEG was used to block nonspecific binding sites on the surface of metal nanoparticles for preventing nonspecific adsorption of the antibody in following reaction [24]. PBS containing PEG (0.05%, w/v) was used in the following steps unless otherwise indicated. And then, a given of antibody was added the solution above, the solution was stirred for 2 min and reacted for 2 h at room temperature and 12 h at 4 °C. The final SNPs–antibody was centrifuged to remove unbound antibody in suspension. The deposition was redissolved in PBS and was stored at 4 °C for use within one week. We obtained two different molar ratio (SNPs/antibody) SNPs–antibody conjugates by controlling the molar ratio of SNPs/antibody in conjugation process.

2.6. Immune reaction

All immune reactions were preformed in PBS containing PEG and all vessels including pipettes, tips and the coverslip were sterilized strictly. The mixture of Alexa Fluor 647-labeled antigen (AFP) and SNPs–antibody conjugates (2:1 and 6:1 molar ratios for low-antibody–SNPs conjugate and high-antibody–SNPs conjugate respectively) was incubated at 37 °C for 30 min to form the SNPs–antibody–fluorescent-labeled AFP complex (SAFAC). The SAFAC solution was stored at 4 °C. In competitive immunoassay, the unlabeled AFP reacted with the SAFAC to release the dye-labeled AFP. With the increase of the unlabeled AFP, the SAFAC concentration would decrease and the dye-labeled AFP concentration would increase in solution. Experimentally, a given of unlabeled AFP and SAFAC prepared freshly were mixed gently and incubated for another 30 min at 37 °C, and then about 30 μL sample was subjected to FCS measurements immediately. The measuring time per sample was 120 s.

2.7. FCS measurements

FCS measurements were carried on a home-built FCS system similar to the previously reported setup [45]. In brief, an inverted fluorescence microscope (IX71, Olympus, Japan) was used as the optical system. He–Ne laser with 632.8 nm wavelength (Hongyang Laser Co., Shanghai, China) was reflected by a dichroic mirror (650 DRLP, Omega Optical, USA), and then focused into the sample solution by a water immersion objective (UplanApo, 60 × NA1.2, Olympus, Japan). About 30 μL sample was placed on a coverslip. The fluorescence emission was filtered by a band-pass filter (682DF20, Omega Optical, USA), and lastly, was collected after passing the 65 μm pinhole by avalanche photodiodes (SPCM-AQR14, PerkinElmer EG&G, Canada). The yielded signals were tracked and correlated by a real time correlator (Flex02-12D/C, Correlator.com, USA). The measuring time per sample was 60–120 s.

2.8. Data analysis

For fluorescent particles diffusing in a three-dimensional Gaussian volume element, FCS function is expressed according to Eq. (1) [13–15]

$$G(\tau) = \frac{1}{N} \cdot \left(1 + \frac{T_t e^{-\tau/\tau_{triplet}}}{1 - T_t}\right) \cdot \frac{1}{\left(1 + \frac{\tau}{\tau_D}\right)} \cdot \frac{1}{\sqrt{1 + \left(\frac{\omega_0}{z_0}\right)^2 \cdot \frac{\tau}{\tau_D}}} \quad (1)$$

All obtained FCS data were analyzed with the standard equation for particles diffusing in a three-dimensional Gaussian volume element and nonlinearly fitted with the Origin 6.1 software package based on the Levenberg–Marquardt algorithm. This fit is based on two-component model as following [11,17,18,22]:

$$G(\tau) = \frac{1}{N}\left(1 - T_t + T_t \exp\left(\frac{-\tau}{\tau_{triplet}}\right)\right)\left(\frac{1 - Y}{\left(1 + \frac{\tau}{\tau_{free}}\right)\sqrt{1 + \frac{\omega_0^2}{Z_0^2}\frac{\tau}{\tau_{free}}}} + \frac{Y}{\left(1 + \frac{\tau}{\tau_{bound}}\right)\sqrt{1 + \frac{\omega_0^2}{Z_0^2}\frac{\tau}{\tau_{bound}}}}\right) \quad (2)$$

Where Y denotes the bound ratio of the antibody to the antigen, if $Y = 0$, the Eq. (2) denotes single-component model. τ_{free} and τ_{bound} are the characteristic diffusion times of the free Alexa Fluor 647-labeled antigen and the SNPs–antibody–antigen complex.

2.9. Resonance light scattering correlation spectroscopy (RLSCS)

The principle and set of RLSCS are similar to that of FCS on the basis of the effect of resonance light scattering (RLS) of metal nanoparticles. Like FCS, RLSCS offers scattering light intensities and characteristic diffusion time of metal nanoparticles such as GNPs, as well as other information obtained by autocorrelation function [42]. Herein, RLSCS was used to characterize the modification of SNPs and conjugation of SNPs with antibody. In RLSCS, argon ion

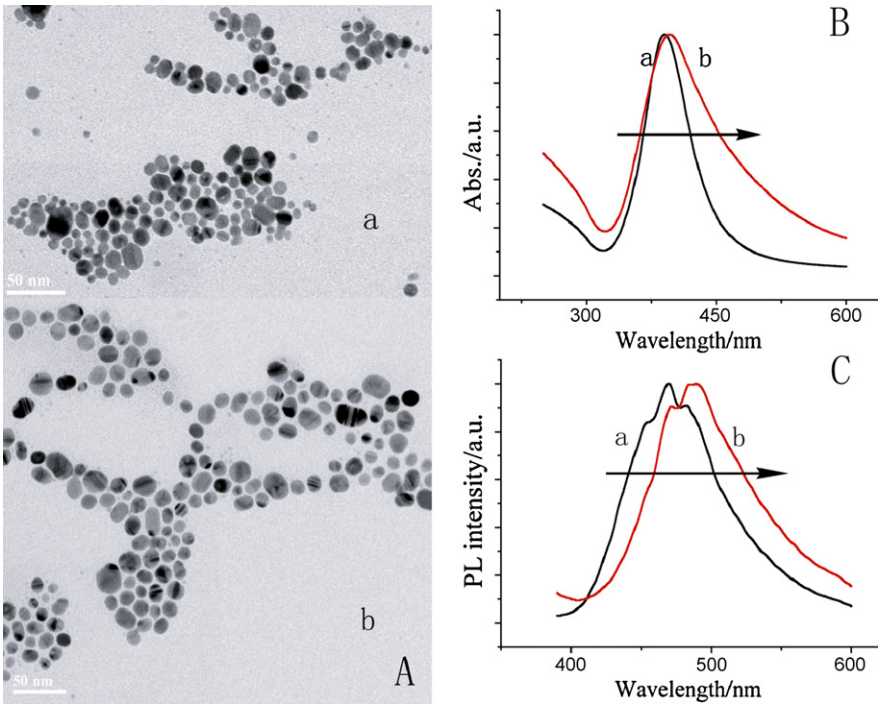

Fig. 2. The absorption spectra, resonance scattering spectra and TEM image of SNP (a) and SNP–MUA (b). (A) The TEM of SNPs (a) and SNP–MUA (b). The detection diameters of them were 14 ± 8 nm, and 15 ± 4 nm respectively. The purification by centrifugation could improve the uniformity of SNPs. (B) UV–vis spectra of SNPs (a) and SNPs–MUA (b). The maximum absorption of SNPs–MUA was red shift by 5.8 nm. (C) Resonance scattering spectra of 14-nm-diameter SNPs (a) and SNPs–MUA (b). Their maximum scattering of SNPs (a) and SNP–MUA (b) were at about 470 nm and 489 nm.

laser (488 nm) was used as light source since the maximum resonance scattering of 14 nm SNPs was at about 470 nm (Fig. 2). The setup of RLSCS in this study was similar to the previously reported system [42]. The setup of RLSCS is also based on an inverted Olympus IX 71 microscope (Olympus, Japan), which is similar to FCS. In brief, an argon ion laser with 488 nm wavelength (Shanghai Ion Laser Co., China) was reflected by a dichroic mirror (505DRLP, Omega Optical, USA), and then focused into the sample solution by a water immersion objective (UplanApo, 60 × NA1.2, Olympus, Japan). The sample was placed on a coverslip (thickness: 170 μm). The scattering signal was collected after passing the 35 μm pinhole by an avalanche photodiode (SPCM-AQR16, PerkinElmer EG&G, Canada). The signals obtained were recorded by a real time digital collector (Flex02-12D/C, Correlator.com, USA). The recording time per sample was 120 s.

3. Results and discussions

3.1. Surface modification of SNPs and conjugation of SNPs to antibody

SNPs were synthesized according to the procedure described in the references [24,44]. The absorption spectra, resonance scattering spectra and TEM image of the as-prepared SNPs were shown in Fig. 2. These characterization results documented that the size of SNPs was about 14 nm, and the maximum resonance scattering and maximum absorption of SNPs were at about 470 nm and 390 nm, respectively. The as-prepared SNPs were well dispersed in aqueous solution. In this study, MUA was used as surface ligands for modification of SNPs since MUA was a good linking bridge contained a thiol group and a carboxyl group, respectively. MUA could easily conjugate to SNPs surface via SNP–S bond. The carboxyl group on MUA modified SNPs could be linked with the amino groups on biomolecules such as proteins, antibodies and peptides [24]. TEM showed that the size of MUA–SNPs was about 15 nm, and the maximum resonance scattering and maximum absorption of MUA–SNPs were red shift by about 19 nm and 5.8 nm, respectively (Fig. 2). The modification of SNPs with MUA was also characterized by RLSCS technique. Fig. 3A and B show the RLSCS curves and the photon burst trajectories of SNPs in the absence of and in the presence of MUA. Like FCS, the correlation time reflects the hydrodynamic radii of diffusing nanoparticles in RLSCS. As seen in Fig. 3A, the correlation time of MUA–SNPs (1.33 ± 0.04 ms) was significantly longer than that of free SNPs (1.23 ± 0.09 ms). This result illustrated that SNPs were successfully modified with MUA. We investigated the effects of MUA concentration and the reaction time on the modification of SNPs and the data are shown in Fig. 3C and D. Interestingly, the correlation time of MUA–SNPs first decreased and then increased with an increase of MUA concentration. This phenomenon was probably attributed to the formation of few dimers or oligmers in the as-prepared SNPs solution. With an increase of MUA concentration, theses dimers or oligmers in solution were dissociated into single nanoparticles, which resulted in the decrease in the correlation time of MUA–SNPs. With the further increase of MUA, more and more MUA molecules were self-organized to the surface of SNPs. The hydrodynamic radii of SNPs gradually enlarged and the correlation time of SNPs prolonged with the increase of MUA concentration. The tendency of the reaction time effect on the modification of SNPs was similar to that of MUA concentration, the correlation time of MUA–SNPs first decreased and then increased with the prolonging of the reaction time. The reason was likely same as the mentions above. Furthermore, we observed that the MUA–SNPs solution was very stable and no aggregates formed for at least 3 weeks, which was confirmed by RLSCS technique.

MUA–SNPs were covalently linked with antibody using EDC and Sulfo-NHS as link reagents. The linkage of MUA–SNPs with antibody was characterized by RLSCS technique. We investigated SNPs–antibody conjugations in different molar ratios of SNPs/antibody (1:2, 1:10, 1:50 and 1:100). The RLSCS curves of SNPs–antibody conjugates are shown in Fig. 4A. The corre-

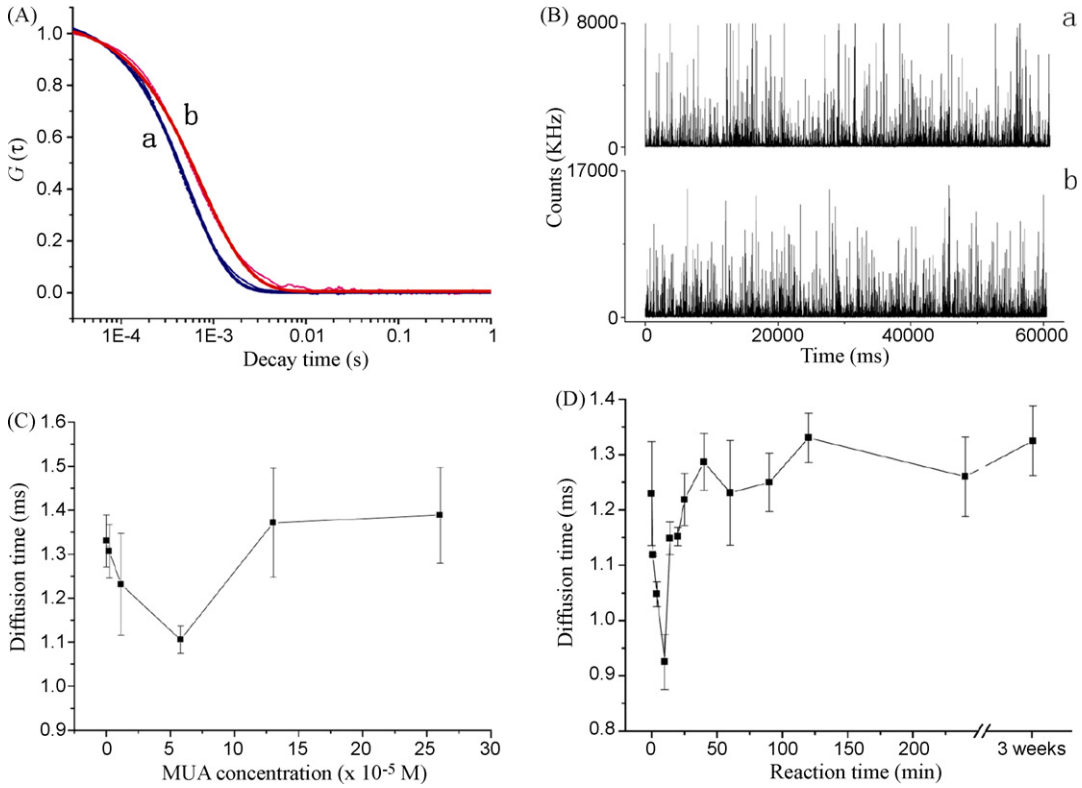

Fig. 3. Surface modification of SNPs with MUA. (A) Normalized RLSCS curves of SNPs (a) and SNPs–MUA (b). (B) The photon counts traces of SNPs (a) and SNPs–MUA (b). (C) The relationship between SNPs–MUA characteristic diffusion time and MUA concentration (0 μM, 2.3 μM, 11.6 μM, 57.9 μM, 130.2 μM and 260.4 μM). (D) The relationship between SNPs–MUA characteristic diffusion time and reaction time (1 min, 4 min, 10 min, 14 min, 20 min, 25 min, 40 min, 60 min, 90 min, 120 min and 240 min), and the results of long-term store samples indicated no aggregation of MUA–SNPs in solution. All samples were measured five times using RLSCS.

lation times of the conjugates were 1.44 ± 0.08 ms (a, black), 1.60 ± 0.09 ms (b, red), 1.76 ± 0.14 ms (c, blue) and 2.96 ± 0.22 ms (d, green), respectively. The correlation times of the conjugates significantly increased with the increase of antibody concentration. This result documented that antibodies were successfully conjugated to SNPs. We also observed that the burst counts decreased with antibody concentration as shown in Fig. 4B. When the molar ratio of SNP–MUA/antibody was 1:2 (sample a), the burst counts of SNP–antibody conjugates was close to that of SNP–MUA. In this case, we called this complex as low-antibody–SNPs conjugates. Further increase of antibody resulted in the conjugation of single SNPs with multiple antibodies, and thus we called this complex as high-antibody–SNPs conjugates (such as sample b). We observed that in the high concentration of the antibody (such as samples c and d), the aggregation of SNPs occurred, which were not suitable for immunoassay. The reason was probably due to the formation of the crosslink structure of multiple SNPs–antibodies conjugates.

3.2. Immune reaction of SNPs–antibody and fluorescent-labeled AFP fluorescence

SNPs–antibody–fluorescent labeled AFP complexes (SAFACs) were prepared by the immune reaction of dye-labeled antigen and SNP–antibody conjugates. As described in the experiment section, we prepared low-antibody–SNPs and high-antibody–SNPs conjugates by controlling the molar ratio of SNPs/antibody in con-

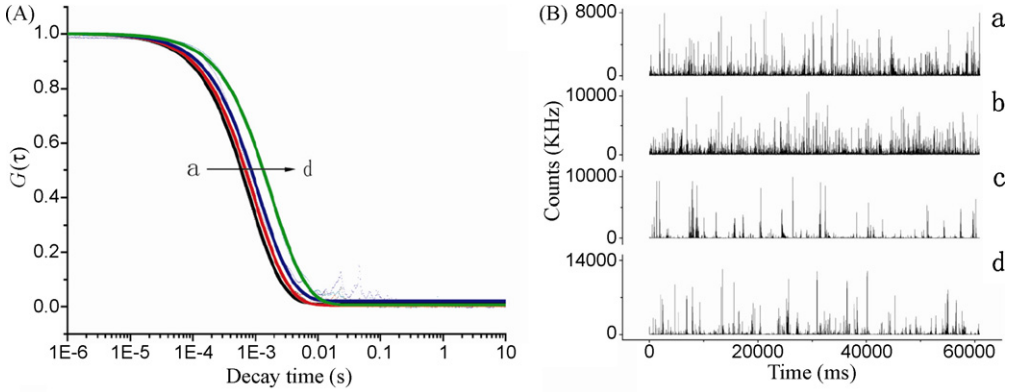

Fig. 4. Conjugation of SNPs to antibody. (A) Normalized RLSCS curves of four kinds of SNP–antibody conjugations (a–d) by controlling the molar ratio of SNPs/antibody in conjugation process. Their molar ratios were 1:2 (a, black), 1:10 (b, red), 1:50 (c, blue) and 1:100 (d, green), respectively. (B) The photon counts traces of four nanoparticles mentioned above. All samples were measured five times using RLSCS. (For interpretation of the references to color in this figure legend, the reader is referred to the web version of the article.)

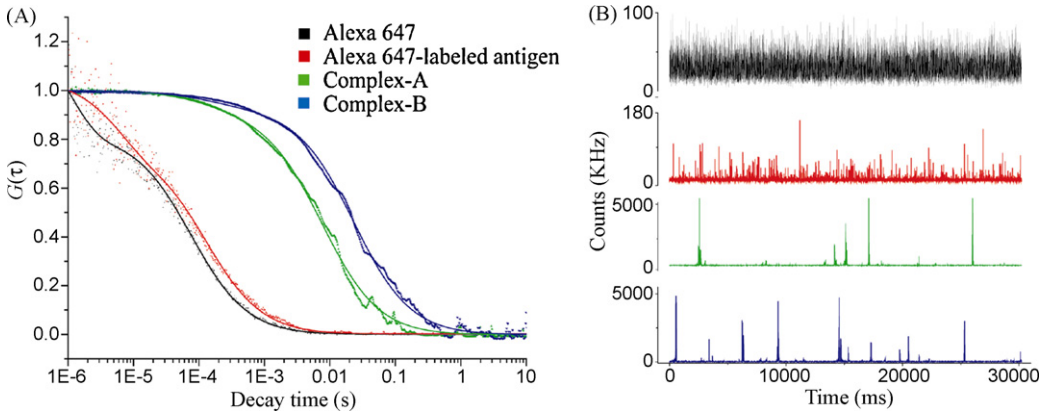

Fig. 5. FCS curves of free Alexa 647, Alexa 647-labeled antigen and SAFACs (Complex-A and Complex-B). (A). Normalized fluorescence correlation curves of Alexa 647 (10 nM), Alexa 647 labeled antigen (180 pM), low-antibody SAFACs (Complex-A, 60 pM) and high-antibody SAFACs (Complex-B, 60 pM). (B) The photon counts traces of four nanoparticles above-mentioned. The SAFACs were synthesized by the affinity of Alexa 647-labeled antigen and SNP–antibody conjugates, which were mixed gently and incubated for 30 min at 37 °C.

jugation process. The immune reaction of SNPs–antibody with fluorescent-labeled AFP was characterized by FCS technique. Fig. 5A shows the correlation curves of Alexa 647 (10 nM), Alexa 647 labeled AFP (180 pM), low-antibody SAFACs (Complex-A, 60 pM) and high-antibody SAFACs (Complex-B, 60 pM). The correlation time of labeled antigen was 0.13 ± 0.01 ms, and two SAFACs were 7.69 ± 0.76 ms and 16.21 ± 3.62 ms, respectively. The results documented that the antigen–antibody complexes showed the increase of about 60-fold (low-antibody–SNPs conjugates) and 120-fold (high-antibody–SNPs conjugates) in the diffusion times compared to free dye-labeled antigen. Such significant difference not only illustrated that the dye-labeled AFP had a strong affinity to SNPs–antibodies conjugates, but also indicated that these immune system satisfied the need of FCS two-component assay model. Larger difference in diffusion behavior of the Complex-B due to the high antibody content would make it to be more sensitive in the FCS assay.

In FCS system, He–Ne laser with 632.8 nm was used as an excitation source. To eliminate the effects of SNPs scattering light, the fluorescence of the Alexa 647-labeled antigen and SAFACs were collected through a bandpass filter (670–692 nm) [28]. Fig. 5B displayed the photon burst trajectories of free dye, labeled AFP and two SAFACs. We observed an obvious enhancement of the fluorescent signal of SAFACs compared to free dye-labeled antigen. This effect could be observed from the intensities of the photon bursts of SAFACs and dye-labeled antigen. The burst intensity of Alexa 647-labeled antigen and the Complex-A were 39.9 ± 1.9 KHz and 745.2 ± 25.8 KHz, resulting in 18.7-fold in fluorescence increase and about 10-fold increase in the signal-to-noise ratio (S/N). Furthermore, the Complex-B showed about 49-fold in fluorescence increase compared to Alexa 647-labeled antigen, and even 2.63-fold increase compared to the Complex-A, which resulted about 20-fold increase in the S/N. The dye-labeled antigen and immune complex could be distinguished easily due to their significant difference of fluorescent intensity. This should be attributable to MEF effects [37,38].

We also investigated the immune reaction of the dye-labeled antigen and SNP–antibody conjugates. The titration curves of dye-labeled antigen with SNP–antibody conjugates are shown in Fig. 6 using two-component assay model of FCS (the normal titration curves (black) of Complex-A (A) and Complex-B (B)) [11,17,18,22]. Experimentally, we kept at a fixed concentration (60 pM) of dye-labeled antigen and increased from 0 to 150 pM SNP–antibody conjugates. The titration end point of the Complex-A and Complex-B systems were 23.5 ± 3.8 pM and 11.1 ± 3.6 pM respectively. Furthermore, dye-labeled antigen (the concentration increased from 0 to 500 pM) was titrated into the SNP–antibody conjugates solution (Complex-A 30 pM, Complex-B 15 pM), and the

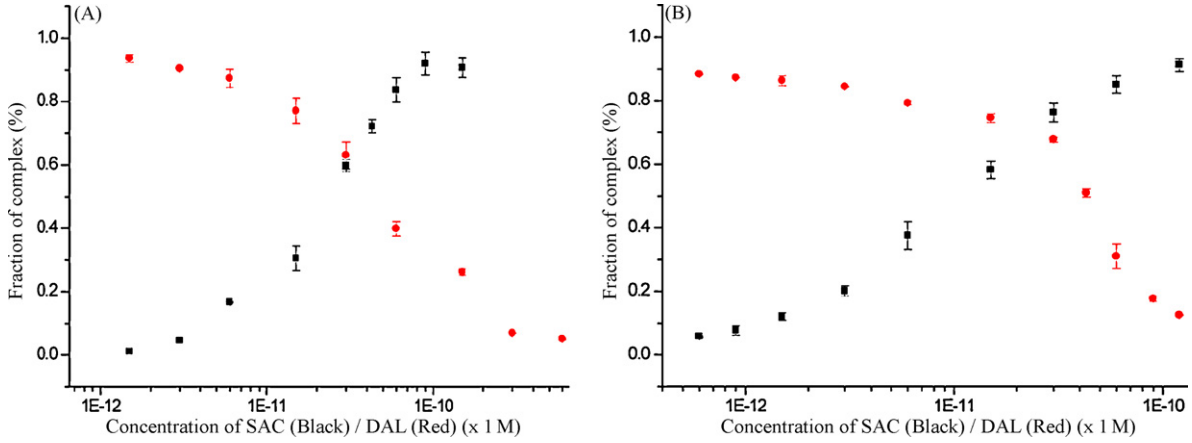

Fig. 6. The normal titration (black) and the inverse-titration (red) curves of Complex-A (A) and Complex-B (B) ($n = 5$, detection time of 2 min). The fraction (%) of SAFACs represented the faction of fluorescence immune complex (SAFACs), and the titration and the inverse-titration curves displayed the relationships between the fraction (%) of SAFACs and SNPs–antibody conjugations (SAC) and dye-labeled antigen (DLA) concentrations. The fractions of SAFACs were calculated based on two-component model (Eq. (2)). The titration end points were calculated by second order derivative method. (For interpretation of the references to color in this figure legend, the reader is referred to the web version of the article.)

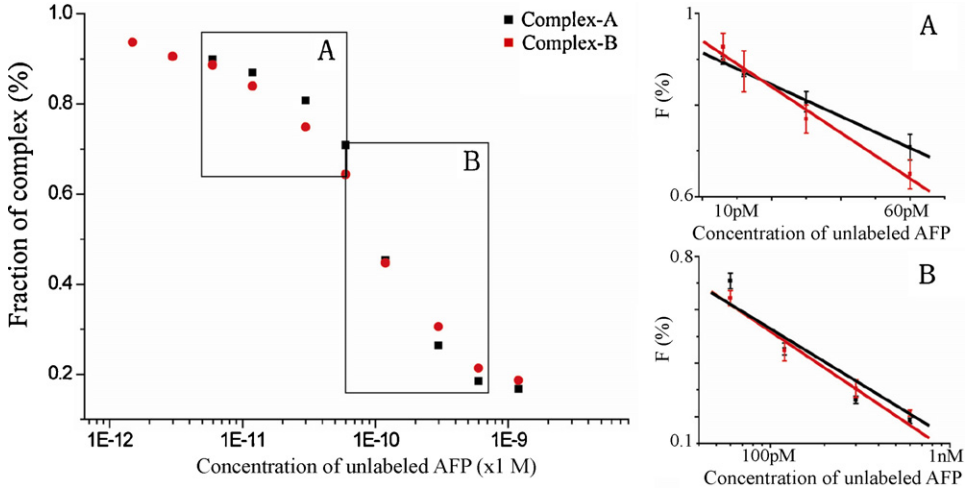

Fig. 7. Titration curves of the competitive immune reaction. Competitive immunoassay was performed by adding unlabeled AFP antigen (concentrations increased from 0 to 1.2 nM) into SAFACs, and the fractions (%) of SAFACs (Complex-A and Complex-B) were calculated by two-component model FCS assay. The fraction of the labeled antigen increased and that of SAFACs decreased with the increase in unlabeled AFP concentration. The detection limits of AFP in Complex-A and Complex-B were 6 pM and 1.5 pM, respectively. The titration curves provided us the calibration curves in two concentration ranges. In the low concentration range (A), the linear range was from 6 pM to 60 pM ($R > 0.99$). In the higher concentration range (B), the linear range was from 60 pM to 600 pM ($R > 0.97$).

inverse-titration curves were obtained. The results are also shown in Fig. 6 (the inverse-titration curves (red) of Complex-A (A) and Complex-B (B)). The inverse-titration end point of the Complex-A and Complex-B systems were 52.9 ± 7.0 pM and 91.6 ± 6.7 pM, respectively.

3.3. Competitive immunoassay

In competitive immunoassay, unlabeled antigen (the concentration increased from 0 nM to 1.2 nM) was mixed with fluorescence immune complex (SAFACs) to release dye-labeled antigen. New immune complex had no signal response in our detection system, which resulted in the decease in the fraction of SAFACs with the increase of the unlabeled antigen. Fig. 7 illustrates the titration curves of SAFACs using two-component assay model of FCS. In competitive immune reaction, the Complex-A and Complex-B showed a similar change tendency, but the detection limit in the Complex-B system was as low as 1.5 pM (6 pM for Complex-A system), which was two orders of magnitude sensitive than current homogeneous immunoassay based on FCS technique [22]. The titration curves provided us two linear ranges of calibration curves [22]. In the low concentration (Fig. 7A), the linear range was from 6 pM to 60 pM ($R > 0.99$). In the higher concentration (Fig. 7B), the linear range was from 60 pM to 600 pM ($R > 0.97$).

Such high sensitivity was mainly due to the significant fluorescence enhancement and significantly different correlation time of SAFACs compared to free dye-labeled antigen. Moreover, the Complex-B possessed larger characteristic time differences as mentioned above, which increased the sensitivity in FCS detection. However, the slight aggregation of SNPs had a negative effect on detection reproducibility in Complex-B system. The relative standard deviation (RSD) for inter-assay in the Complex-B system was 7.2% ($n = 5$) and RSD in the Complex-A system was 4.2% ($n = 5$). The RSDs for intra-assay in both systems were less than 5% ($n = 3$).

In current clinical diagnosis, AFP is considered to be a very important biomarker for liver cancer. It was reported that the AFP level of liver caner patients was significantly higher than those of healthy people [46]. The applicability of the present method was tested with human serum samples for AFP level detection, and the calibration curves ($(Y = 0.914–3.559 \times 10^9 C_{AFP})$ for Complex-A, and $(Y = 0.900–4.442 \times 10^9 C_{AFP})$ for Complex-B) ranged from 6 pM to 60 pM was chosen for quantitative analysis due to its good linearity and low concentration detection limit. Three serum samples from healthy volunteers were first diluted 20 times with PBS in order to decrease the viscosity of serum samples, and then FCS was used to measure the AFP levels of samples. According to the calibration curves (Fig. 7A), the obtained results are shown in Table 1. It should be pointed out that the AFP values in Table 1 magnified with 20 times (dilution times) expressed the AFP level in human serum samples, which were in the normal reference range (<about 294 pM) [46]. The RSDs of assays were about 5%. In the recovery experiments, a given unlabeled antigen (12 pM AFP) was added to the serum samples, and the recoveries of AFP are shown in Table 1. Our preliminary experimental data demonstrated that the

Table 1
The recovery results of AFP with human serum samples.

	Original AFP (pM)	RSD (%)	Added AFP (pM)	Measured AFP (pM)	RSD (%)	Recovery (%)
Complex-A system						
Sample 1	8.0	2.2	12.0	18.8	3.5	90.0
Sample 2	7.3	1.8	12.0	18.8	1.9	95.8
Sample 3	8.0	2.3	12.0	19.1	2.3	92.5
Complex-B system						
Sample 1	7.1	4.7	12.0	18.2	5.4	92.5
Sample 2	8.1	5.4	12.0	18.8	5.3	89.2
Sample 3	7.1	1.8	12.0	18.2	2.4	92.5

In recovery experiments, a given amount of AFP (12 pM) was added into human serum after the sample was 20 times diluted with buffer. The AFP concentrations of original serum and mixture samples were measured using silver nanoparticle enhanced fluorescence correlation spectroscopy. The RSDs were derived from five independent experiments.

immunoassay using SNPs enhancement FCS was a sensitive and efficient method for the detection of AFP marker.

4. Conclusion

In this work, we first characterized the modification of SNPs with MUA and conjugation of SNPs with antibody by RLSCS technique, and then investigated the immune reaction of SNPs–antibody and AFP antigen by FCS. In the immunoassay, SNPs were used to enlarge the molecule weight difference between the immunocomplex and antigen, and to enhance the fluorescent intensity of fluoroprobes. On the base of the SNPs effects, we developed the homogeneous competitive immunoassay using the two-component model of FCS analysis. This assay was successfully applied for the determination of the AFP level in normal human serum samples. When compared to current immunoassays, our method can be characterized as high sensitivity, good selectivity, simplicity and short analysis time, and possesses great potential applications in clinical diagnosis, food and environmental analysis and biological and biomedical studies.

Acknowledgements

This work was financially supported by NSFC (20727005, 20975067) and National Basic Research Program of China (2009CB930400).

References

[1] Z. Lin, X. Wang, Z.J. Li, S.Q. Ren, G.N. Chen, X.T. Ying, J.M. Lin, Talanta 75 (2008) 965.
[2] P. Su, X.X. Zhang, Y.C. Wang, W.B. Chang, Talanta 60 (2003) 969.
[3] J.A. Gabaldon, A. Maquieira, R. Puchades, Talanta 71 (2007) 1001.
[4] J. Wang, W. Huang, Y. Liu, J. Cheng, J. Yang, Anal. Chem. 76 (2004) 5393.
[5] Z. Fu, H. Liu, H. Ju, Anal. Chem. 78 (2006) 6999.
[6] K. Aurich, S. Nagel, G. Glockl, W. Weitschies, Anal. Chem. 79 (2007) 580.
[7] C. Xie, F.G. Xu, X.Y. Huang, C.Q. Dong, J.C. Ren, J. Am. Chem. Soc. 131 (2009) 12763.
[8] T. Tachi, N. Kaji, M. Tokeshi, Y. Baba, Lab Chip 9 (2009) 966.
[9] L.Z. Liu, M. Shao, X.H. Dong, X.F. Yu, Z.H. Liu, Z.K. He, Q.Y. Wang, Anal. Chem. 80 (2008) 7735.
[10] F. Fujii, M. Horiuchi, M. Ueno, H. Sakata, I. Nagao, M. Tamura, M. Kinjo, Anal. Biochem. 370 (2007) 131.
[11] O.A. Mayboroda, A. Van Remoortere, H.J. Tanke, C.H. Hokke, A.M. Deelder, J. Biotechnol. 107 (2004) 185.
[12] Z. Foldes-Papp, U. Demel, G.P. Tilz, J. Immunol. Methods 260 (2002) 117.
[13] E. Elson, D. Magde, Biopolymers 13 (1974) 1.
[14] R. Rigler, U. Mets, J. Widengren, P. Kask, Eur. Biophys. J. 22 (1993) 169.
[15] E. Haustein, P. Schwille, Annu. Rev. Biophys. Biomol. Struct. 36 (2007) 151.
[16] J. Ries, S.R. Yu, M. Burkhardt, M. Brand, P. Schwille, Nat. Methods 6 (2009) 643.
[17] S.Y. Tetin, K.M. Swift, E.D. Matayoshi, Anal. Biochem. 307 (2002) 84.
[18] S.Y. Tetin, S.D. Stroupe, Curr. Pharm. Biotechnol. 5 (2004) 9.
[19] Q. Ruan, S.Y. Tetin, Anal. Biochem. 374 (2008) 182.
[20] P. Schwille, F.J. Meyer-Almes, R. Rigler, Biophys. J. 72 (1997) 1878.
[21] A. Barriale, M. Rossi, M. Staiano, E. Terpetschnig, B. Barbieri, M. Rossi, S. D'Auria, Anal. Chem. 79 (2007) 4687.
[22] C. Xie, C.Q. Dong, J.C. Ren, Talanta 79 (2009) 971.
[23] H. He, C. Xie, J.C. Ren, Anal. Chem. 80 (2008) 5951.
[24] T. Huang, P.D. Nallathamby, D. Gillet, X.N. Xu, Anal. Chem. 79 (2007) 7708.
[25] J. Zhang, Y. Fu, D. Liang, R.Y. Zhao, J.R. Lakowicz, Anal. Chem. 81 (2009) 883.
[26] J.W. Liu, Y. Lu, J. Am. Chem. Soc. 126 (2004) 12298.
[27] Y. Jiang, H. Zhao, N.N. Zhu, Y.Q. Lin, P. Yu, L.Q. Mao, Angew. Chem. Int. Ed. 47 (2008) 8601.
[28] K. Ray, J. Zhang, J.R. Lakowicz, Anal. Chem. 80 (2008) 7313.
[29] D.G. Thompson, A. Enright, K. Faulds, W.E. Smith, D. Graham, Anal. Chem. 80 (2008) 2805.
[30] H. Surin, I. Choi, S. Lee, Y.I. Yang, T. Kang, J. Yi, Anal. Chem. 81 (2009) 1378.
[31] C. Cao, S.J. Sim, Lab Chip 9 (2009) 1836.
[32] N. Chanda, R. Shukla, K.V. Katti, R. Kannan, Nano Lett. 9 (2009) 1798.
[33] J.R. Lakowicz, Anal. Biochem. 337 (2005) 171.
[34] K. Ray, R. Badugu, J.R. Lakowicz, J. Am. Chem. Soc. 128 (2006) 8998.
[35] K. Ray, M.H. Chowdhury, J.R. Lakowicz, Anal. Chem. 80 (2008) 6942.
[36] J. Zhang, Y. Fu, M.H. Chowdhury, J.R. Lakowicz, Nano Lett. 7 (2007) 2101.
[37] Y. Fu, J. Zhang, J.R. Lakowicz, Chem. Commun. 3 (2009) 313.
[38] J. Zhang, Y. Fu, M.H. Chowdhury, J.R. Lakowicz, J. Phys. Chem. C 112 (2008) 9172.
[39] K. Ray, R. Badugu, J.R. Lakowicz, J. Phys. Chem. C 111 (2007) 7091.
[40] Y. Fu, J. Zhang, J.R. Lakowicz, Biochem. Biophys. Res. Commun. 376 (2008) 712.
[41] J. Ling, Y.F. Li, C.Z. Huang, Anal. Chem. 81 (2009) 1707.
[42] K.L. Wang, X. Qiu, C.Q. Dong, J.C. Ren, ChemBioChem 8 (2007) 1126.
[43] G.I. Abelev, Cancer Res. 28 (1968) 1344.
[44] L. Lu, A. Kobayashi, K. Tawa, Y. Ozaki, Chem. Mater. 18 (2006) 4894.
[45] P.D. Zhang, C.Q. Dong, H.F. Qian, J.C. Ren, Anal. Chim. Acta. 546 (2005) 46.
[46] J.R. Bloomer, Digest. Dis. Sci. 25 (1980) 241.